Lecture Notes in Electrical Engineering 1205

Qing Wang
Xiwang Dong
Peng Song *Editors*

Proceedings of 2023 7th Chinese Conference on Swarm Intelligence and Cooperative Control

Swarm Control Technologies

Springer

Lecture Notes in Electrical Engineering 1205

The book series *Lecture Notes in Electrical Engineering* (LNEE) publishes the latest developments in Electrical Engineering—quickly, informally and in high quality. While original research reported in proceedings and monographs has traditionally formed the core of LNEE, we also encourage authors to submit books devoted to supporting student education and professional training in the various fields and applications areas of electrical engineering. The series cover classical and emerging topics concerning:

- Communication Engineering, Information Theory and Networks
- Electronics Engineering and Microelectronics
- Signal, Image and Speech Processing
- Wireless and Mobile Communication
- Circuits and Systems
- Energy Systems, Power Electronics and Electrical Machines
- Electro-optical Engineering
- Instrumentation Engineering
- Avionics Engineering
- Control Systems
- Internet-of-Things and Cybersecurity
- Biomedical Devices, MEMS and NEMS

For general information about this book series, comments or suggestions, please contact leontina.dicecco@springer.com.

To submit a proposal or request further information, please contact the Publishing Editor in your country:

China

Jasmine Dou, Editor (jasmine.dou@springer.com)

India, Japan, Rest of Asia

Swati Meherishi, Editorial Director (Swati.Meherishi@springer.com)

Southeast Asia, Australia, New Zealand

Ramesh Nath Premnath, Editor (ramesh.premnath@springernature.com)

USA, Canada

Michael Luby, Senior Editor (michael.luby@springer.com)

All other Countries

Leontina Di Cecco, Senior Editor (leontina.dicecco@springer.com)

**** This series is indexed by EI Compendex and Scopus databases. ****

Qing Wang · Xiwang Dong · Peng Song
Editors

Proceedings of 2023 7th Chinese Conference on Swarm Intelligence and Cooperative Control

Swarm Control Technologies

Springer

Editors
Qing Wang
School of Automation Science and Electrical Engineering
Beihang University
Beijing, China

Xiwang Dong
Institute of Artificial Intelligence
Beihang University
Beijing, China

Peng Song
Chinese Institute of Command and Control
Beijing, China

ISSN 1876-1100 ISSN 1876-1119 (electronic)
Lecture Notes in Electrical Engineering
ISBN 978-981-97-3327-9 ISBN 978-981-97-3328-6 (eBook)
https://doi.org/10.1007/978-981-97-3328-6

This Springer imprint is published by the registered company Springer Nature Singapore Pte Ltd.
The registered company address is: 152 Beach Road, #21-01/04 Gateway East, Singapore 189721, Singapore

Contents

Inter-layer Generalized Synchronization for Fractional-Order Two-Layer Networks Based on Auxiliary-System Method

Xiong Wang[1](✉) and Haibo Gu[2]

[1] The School of Mathematics, Northwest University, Xi'an, China
xiongwang@nwu.edu.cn

[2] The School of Automation Science and Electrical Engineering, Beihang University, Beijing, China

Abstract. This paper focuses on investigating inter-layer generalized synchronization for fractional-order two-layer networks, the two layers in which have nonidentical node dynamics, different topologies, and unknown functional relationships. On the basis of the auxiliary-system method, an auxiliary system is constructed, specifically, the auxiliary system and the response (bottom) layer receive the same control inputs from the drive (top) layer. In addition, the adaptive controllers are designed to ensure the bottom layer and the auxiliary layer to realize complete synchronization. The top layer achieves inter-layer generalized synchronization with the bottom layer simultaneously. Eventually, numerical examples are conducted to verify the effectiveness of our established synchronization method.

Keywords: fractional-order two-layer networks · generalized synchronization · auxiliary-system method

1 Introduction

As a powerful tool for explaining and analyzing the coordination phenomena in the real-world systems, synchronization of complex networks have penetrated many scientific fields such as social, engineering and biological [1]. Thus far, the existing research on synchronization of complex networks mainly focus on integer-order networks [2–5]. However, many real phenomena have genetic and memory characteristics, which are more accurately explained by fractional order dynamics, for instance, random diffusion, viscoelastic materials, to name a few [6,7]. Thus, it is urgent to mine novel theoretical frameworks and approaches for fractional-order networks.

Recently, scholars have mostly devoted themselves to investigating the synchronization method of single-layer fractional-order complex networks [8–10]. Yet many real industrial and social networks include multiple layers of connectivity. Ref. [11,12] studied synchronization and finite-time synchronization for fractional-order multi-weighted networks. However, the above works did not take into account the coupling relationship between different layers in multilayer networks. In 2020, Zhang *et al.* explored

Q. Wang et al. (Eds.): CCSICC 2023, LNEE 1205, pp. 1–10, 2024.
https://doi.org/10.1007/978-981-97-3328-6_1

intralayer and interlayer synchronization for fractional-order two-layer networks by adjusting the coupling strengths [13]. Subsequently, Wu *et al.* investigated finite-time synchronization of fractional-order two-layer and multilayer networks via sliding mode and adaptive control, respectively [14, 15]. In 2022, Luo *et al.* presented asymptotic synchronization and finite-time synchronization methods for fractional-order multilayer networks by designing adaptive and impulsive controllers [16].

It is worth noting that the aforementioned works primarily concentrated on complete synchronization [11–13, 15, 16] or inter-layer projective synchronization [14]. These works assumed that nodes in different layers of multilayer networks have exactly identical or proportional dynamics, even the designed controllers are usually complicated. Nevertheless, in practical applications, as is known to all that nodes in different layers always have different dynamics [17]. For instance, in communication-epidemic spreading networks, two layers behave in diversely ways and have nonidentical node dynamics. Therefore, it is crucial to design a simpler controller to realize synchronization for two-layer networks with nonidentical node dynamics in different layers.

Motivated by the previous discussions, this article aims to investigate inter-layer generalized synchronization for fractional-order two-layer networks. Considering nodes between two layers have nonidentical dynamics, different topologies, and the unknown functional relationships, an auxiliary layer is constructed. And then, some adaptive controllers are designed such that the auxiliary system and the bottom layer of fractional-order two-layer networks reach complete outer synchronization. As the auxiliary-system method [17], the top layer and the bottom layer realize inter-layer generalized synchronization simultaneously. Our proposed method is simple and effective.

2 Preliminaries

In this section, some necessary definitions, properties, and assumptions are introduced, moreover, our model is constructed.

Definition 1 [6]. *The fractional integral of a function $\omega(\cdot)$ is defined by*

$$ {}_{t_0}I_t^{\alpha}\omega(t) = \frac{1}{\Gamma(\alpha)} \int_{t_0}^{t} (t-s)^{\alpha-1}\omega(s)ds, $$

where $0 \leq t_0 < t$, $\alpha \in (0,1)$, $\Gamma(\alpha) = \int_0^{\infty} t^{\alpha-1}e^{-t}dt$ is the gamma function.

Definition 2 [6]. *The Caputo fractional derivative for a function $\omega(\cdot)$ is defined by*

$$ {}_{t_0}^{C}D_t^{\alpha}\omega(t) = \frac{1}{\Gamma(1-\alpha)} \int_{t_0}^{t} \frac{\omega'(s)}{(t-s)^{\alpha}}ds, $$

where $0 \leq t_0 < t$, $\alpha \in (0,1)$.

Property 1 [7]. *If $\omega(t) \in C^1[t_0, +\infty)$ and $0 < \alpha \leq 1$, then*

$$ {}_{t_0}I_t^{\alpha}\,{}_{t_0}^{C}D_t^{\alpha}\omega(t) = \omega(t) - \omega(t_0). $$

Property 2 [7]. *If $\omega(t) \in C^1[t_0, +\infty)$, then for $t > t_0$*

$$
{}_{t_0}^{C}D_t^{\alpha}||\omega(t)||_1 \leq sgn(\omega(t)){}_{t_0}^{C}D_t^{\alpha}\omega(t),
$$
$$
{}_{t_0}^{C}D_t^{\alpha}\omega^2(t) \leq 2\omega(t){}_{t_0}^{C}D_t^{\alpha}\omega(t),
$$

where $sgn(\cdot)$ be the symbolic function.

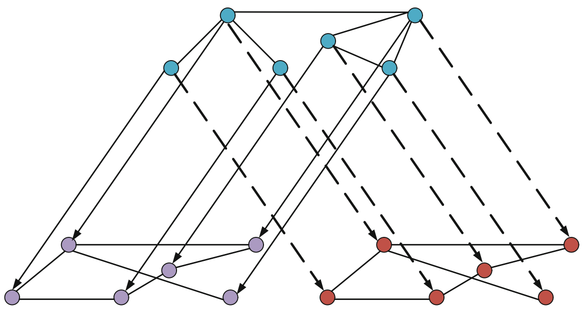

Fig. 1. The schematic diagram of our methods.

Consider a class of unidirectionally coupled fractional-order two-layer networks which consists of N nodes in each layer. The nodes are one-to-one correspondence in the two-layer networks as depicted in Fig. 1, with the node dynamics ($i = 1, 2, ..., N$) be described as

$$
{}_{t_0}^{C}D_t^{\alpha}x_i(t) = f_i(t, x_i(t)) + c_1 \sum_{j=1}^{N} a_{ij}H_1x_j(t), \tag{1}
$$

$$
{}_{t_0}^{C}D_t^{\alpha}y_i(t) = g_i(t, y_i(t)) + c_2 \sum_{j=1}^{N} b_{ij}H_2y_j(t) + u_i(x_i(t), y_i(t)), \tag{2}
$$

In which, system (1) is the network dynamics of the top network (layer), we take it as the drive layer. And system (2) describes that of the bottom layer, which is regarded as the response layer. $x_i(t) \in \mathbb{R}^n$ and $y_i(t) \in \mathbb{R}^n$ are the node states of the ith node at time t ($t \geq t_0$) in the drive (top) network and response (bottom) network, respectively. $f_i, g_i \in \mathbb{R}^n$ are nonlinear functions. $H_1,\ H_2 \in \mathbb{R}^{n\times n}$ and $c_1,\ c_2$ are inner-coupling matrices and coupling strengths of the drive (top) network and response (bottom) network, respectively. $A = (a_{ij})_{N\times N}$ and $B = (b_{ij})_{N\times N} \in \mathbb{R}^{N\times N}$ are outer-coupling matrices of the drive (top) network and response (bottom) network, respectively, which are given as follows: if there exists a link from jth node to i ($i \neq j$)th node in the drive network (the response network), then $a_{ij} \neq 0$ ($b_{ij} \neq 0$), or else, $a_{ij} = 0$ ($b_{ij} = 0$), and $a_{ii} = -\sum_{j=1,j\neq i}^{N} a_{ij}$ $(b_{ii} = -\sum_{j=1,j\neq i}^{N} b_{ij})$. $u_i(x_i(t), y_i(t))$ denotes the control input from the drive network (the top layer) to the response network (the bottom layer).

In order to realize inter-layer generalized synchronization between the response network (the bottom layer) (2) and the drive network (the top layer) (1), according to the auxiliary-system method, an auxiliary system which is similar as the response network (the bottom layer) is constructed as follows

$$ {}_{t_0}^{C}D_t^{\alpha} z_i(t) = g_i(t, z_i(t)) + c_2 \sum_{j=1}^{N} b_{ij} H_2 z_j(t) + u_i(x_i(t), z_i(t)), \tag{3} $$

where $z_i(t) \in \mathbb{R}^n$ is the ith node's state. $u_i(x_i(t), z_i(t))$ be the control input which has the similar form as that of $u_i(x_i(t), y_i(t))$.

Assumption 1. *For any $\theta(t), \vartheta(t) \in \mathbb{R}^n$, the nonlinear functions $g_i(t, \cdot)$ $(i = 1, 2, ..., N)$ satisfy*

$$ ||g_i(t, \theta(t)) - g_i(t, \vartheta(t))||_1 \leq \alpha_i ||\theta(t) - \vartheta(t)||_1, $$

where α_i $(i = 1, 2, ..., N)$ be some positive constants.

Define the error systems for node i between the response network (the bottom layer) (2) and the auxiliary system (3) by

$$ e_i(t) = y_i(t) - z_i(t), \quad i = 1, 2, ..., N. \tag{4} $$

Remark 1. Note that the auxiliary-system method is a technique to monitor the synchronized motions between the response network and the drive network via constructing an auxiliary system. This auxiliary system also receives signals from the drive layer in one direction as the response network. It is said generalized synchronization between the response network and the drive network occurs if the auxiliary system achieve complete outer synchronization with the response network.

As the auxiliary-system method illustrated by Fig. 1, in this paper, we construct an auxiliary system that has identical node dynamics and topologies with the response (bottom) network, and receives control inputs from the drive (top) network in one direction as the response (bottom) network. When the auxiliary system (3) and the response (bottom) layer (2) reach complete outer synchronization, the drive network (the top layer) (1) and the response network (the bottom layer) (2) achieve generalized synchronization simultaneously.

3 Inter-layer Generalized Synchronization for Fractional-Order Two-Layer Networks

In this section, inter-layer generalized synchronization method for fractional-order two-layer networks are exhibited.

Theorem 1. *Suppose Assumption 1 holds, if*

$$\lambda := \min_{1\le i\le N}\{\varphi_i^* - \alpha_i - c_2\sum_{j=1}^{N}|b_{ji}|||H_2||_1\} > 0, \tag{5}$$

then the drive (top) layer (1) achieves inter-layer generalized synchronization with the response (bottom) layer (2) via the following adaptive controllers

$$\begin{aligned} u_i(x_i(t), y_i(t)) &= -\,\varphi_i(t)(y_i(t) - x_i(t)),\\ u_i(x_i(t), z_i(t)) &= -\,\varphi_i(t)(z_i(t) - x_i(t)),\\ {}_{t_0}^{C}D_t^{\alpha}\varphi_i(t) &= \kappa_i||e_i(t)||_1, \quad i = 1, 2, ..., N, \end{aligned} \tag{6}$$

where κ_i be a arbitrary positive constant while φ_i^* be a positive constant to be determined.

Proof. According to the definition of errors (4) and the designed adaptive controllers (6), the error systems can be written by

$$\begin{aligned} {}_{t_0}^{C}D_t^{\alpha}e_i(t) =& {}_{t_0}^{C}D_t^{\alpha}y_i(t) - {}_{t_0}^{C}D_t^{\alpha}z_i(t)\\ &= g_i(t, y_i(t)) - g_i(t, z_i(t)) + c_2\sum_{j=1}^{N} b_{ij}H_2e_j(t) - \varphi_i(t)e_i(t), \\ i =& 1, 2, ..., N. \end{aligned} \tag{7}$$

The following Lyapunov function is considered

$$V(t) = \sum_{k=1}^{N}||e_k(t)||_1 + \sum_{k=1}^{N}\frac{1}{2\kappa_k}(\varphi_k(t) - \varphi_k^*)^2. \tag{8}$$

Calculate the Caputo fractional-order derivatives for $V(t)$ along with solutions of the error systems (7), one gets

$$\begin{aligned} &{}_{t_0}^{C}D_t^{\alpha}V(t)\\ &= \sum_{k=1}^{N}{}_{t_0}^{C}D_t^{\alpha}||e_k(t)||_1 + \sum_{k=1}^{N}\frac{1}{2\kappa_k}{}_{t_0}^{C}D_t^{\alpha}(\varphi_k(t) - \varphi_k^*)^2\\ &\le \sum_{k=1}^{N} sgn^{\mathrm{T}}(e_k(t)){}_{t_0}^{C}D_t^{\alpha}e_k(t) + \sum_{k=1}^{N}\frac{1}{\kappa_k}(\varphi_k(t) - \varphi_k^*){}_{t_0}^{C}D_t^{\alpha}\varphi_k(t)\\ &= \sum_{k=1}^{N} sgn^{\mathrm{T}}(e_k(t)){}_{t_0}^{C}D_t^{\alpha}e_k(t) + \sum_{k=1}^{N}(\varphi_k(t) - \varphi_k^*)||e_k(t)||_1\\ &= \sum_{k=1}^{N} sgn^{\mathrm{T}}(e_k(t))\Big(g_k(t, y_k(t)) - g_k(t, z_k(t)) + c_2\sum_{j=1}^{N} b_{kj}H_2e_j(t) - \varphi_k(t)e_k(t)\Big)\\ &\quad + \sum_{k=1}^{N}(\varphi_k(t) - \varphi_k^*)||e_k(t)||_1\\ &= \sum_{k=1}^{N}\Big(sgn^{\mathrm{T}}(e_k(t))\big(g_k(t, y_k(t)) - g_k(t, z_k(t)) + c_2\sum_{j=1}^{N} b_{kj}H_2e_j(t)\big) - \varphi_k^*||e_k(t)||_1\Big). \end{aligned}$$

Recall Assumption 1 and Property 2, one has

$$\begin{aligned}
&\sum_{k=1}^{N} sgn^{\mathrm{T}}(e_k(t))\Big(g_k(t,y_k(t))-g_k(t,z_k(t))\Big)\\
&=\sum_{k=1}^{N}\sum_{l=1}^{n} sgn(e_{kl}(t))\Big(g_{kl}(t,y_k(t))-g_{kl}(t,z_k(t))\Big)\\
&\leq\sum_{k=1}^{N}\sum_{l=1}^{n} |sgn(e_{kl}(t))||g_{kl}(t,y_k(t))-g_{kl}(t,z_k(t))|\\
&\leq\sum_{k=1}^{N}\sum_{l=1}^{n} |g_{kl}(t,y_k(t))-g_{kl}(t,z_k(t))|\\
&=\sum_{k=1}^{N} ||g_k(t,y_k(t))-g_k(t,z_k(t))||_1\\
&\leq\sum_{k=1}^{N} \alpha_k||e_k(t)||_1,
\end{aligned} \tag{9}$$

and

$$\begin{aligned}
&\sum_{k=1}^{N} sgn^{\mathrm{T}}(e_k(t))\sum_{j=1}^{N} b_{kj}H_2e_j(t)\\
&=\sum_{k=1}^{N} b_{kk}H_2||e_k(t)||_1+\sum_{k=1}^{N}\sum_{j=1,j\neq k}^{N} sgn^{\mathrm{T}}(e_k(t))b_{kj}H_2e_j(t)\\
&=\sum_{k=1}^{N} b_{kk}H_2||e_k(t)||_1+\sum_{j=1}^{N}\sum_{k=1,j\neq k}^{N} sgn^{\mathrm{T}}(e_j(t))b_{jk}H_2e_k(t)\\
&\leq\sum_{k=1}^{N} b_{kk}H_2||e_k(t)||_1+\sum_{j=1}^{N}\sum_{k=1,j\neq k}^{N} |b_{jk}|\sum_{p=1}^{n}\sum_{q=1}^{n}|H_2^{pq}||e_{kq}|\\
&\leq\sum_{k=1}^{N} b_{kk}H_2||e_k(t)||_1+\sum_{j=1}^{N}\sum_{k=1,j\neq k}^{N} |b_{jk}|\max_{1\leq q\leq n}\Big(\sum_{p=1}^{n}|H_2^{pq}|\Big)\sum_{q=1}^{n}|e_{kq}(t)|\\
&=\sum_{k=1}^{N} b_{kk}H_2||e_k(t)||_1+\sum_{j=1}^{N}\sum_{k=1,j\neq k}^{N} |b_{jk}|||H_2||_1||e_k(t)||_1\\
&\leq\sum_{k=1}^{N}\sum_{j=1}^{N} |b_{jk}|||H_2||_1||e_k(t)||_1.
\end{aligned} \tag{10}$$

Together with inequalities (5), (9), and (10), which can be demonstrated that

$$\begin{aligned}
{}_{t_0}^{C}D_t^{\alpha}V(t) \leq & \sum_{k=1}^{N}\left(\alpha_k + c_2\sum_{j=1}^{N}|b_{jk}|||H_2||_1 - \varphi_k^*\right)||e_k(t)||_1 \\
= & -\sum_{k=1}^{N}\left(\varphi_k^* - \alpha_k - c_2\sum_{j=1}^{N}|b_{jk}|||H_2||_1\right)||e_k(t)||_1 \\
\leq & -\lambda\sum_{k=1}^{N}||e_k(t)||_1.
\end{aligned} \tag{11}$$

Let $W(t) = \sum_{i=1}^{N}||e_i(t)||_1 > 0$, which yields that ${}_{t_0}^{C}D_t^{\alpha}V(t) \leq -\lambda W(t)$. According to Definition 1 and Property 1, one can deduce that

$$V(t) - V(t_0) \leq \frac{1}{\Gamma(\alpha)}\int_{t_0}^{t}(t-s)^{\alpha-1}\big(-\lambda W(s)\big)ds \leq 0.$$

It indicates that $V(t)$ is bounded. Form the definition of $V(t)$ in (8), $e_i(t), \varphi_i(t)$, and $W(t)$ are bounded on $t > t_0 \geq 0$. According to error system (7), ${}_{t_0}^{C}D_t^{\alpha}e_i(t)$ is bounded.

In the following, the contradiction method will be adopted to prove $\lim_{t\to+\infty}W(t) = 0$. Otherwise, assume that $\lim_{t\to+\infty}W(t) = \beta > 0$.

For $\forall\,\varepsilon > 0,\ \exists\,t^*,\ \forall\,t > t^*$, one gets

$$|W(t) - \beta| < \varepsilon,$$

when $\varepsilon = \beta/2$, one has

$$0 < \frac{\beta}{2} < W(t) < \frac{3\beta}{2}, \quad \forall\,t > t^*. \tag{12}$$

Therefore, one obtains

$$\begin{aligned}
V(t) - V(t_0) = & \ {}_{t_0}I_t^{\alpha}\,{}_{t_0}^{C}D_t^{\alpha}V(t) \\
= & \frac{1}{\Gamma(\alpha)}\int_{t_0}^{t}(t-s)^{\alpha-1}\,{}_{t_0}^{C}D_t^{\alpha}V(t)ds \\
= & \frac{1}{\Gamma(\alpha)}\left(\int_{t^*}^{t}(t-s)^{\alpha-1}\,{}_{t_0}^{C}D_t^{\alpha}V(s)ds + \int_{t_0}^{t^*}(t-s)^{\alpha-1}\,{}_{t_0}^{C}D_t^{\alpha}V(s)ds\right),
\end{aligned}$$

due to ${}_{t_0}^{C}D_t^{\alpha}V(s) \leq 0$, then one obtains

$$\begin{aligned}
V(t) - V(t_0) \leq & \frac{1}{\Gamma(\alpha)}\int_{t^*}^{t}(t-s)^{\alpha-1}\,{}_{t_0}^{C}D_t^{\alpha}V(s)ds \\
\leq & \frac{1}{\Gamma(\alpha)}\int_{t^*}^{t}(t-s)^{\alpha-1}\big(-\lambda W(s)\big)ds \\
< & -\frac{\lambda\beta}{2\Gamma(\alpha)}\int_{t^*}^{t}(t-s)^{\alpha-1}ds \\
= & -\frac{\lambda\beta}{2\Gamma(\alpha+1)}(t-t^*)^{\alpha},
\end{aligned}$$

which reveals that $\lim_{t\to+\infty} V(t) < -\infty$, it contradicts with the fact $V(t) \geq 0$. Therefore, $\lim_{t\to+\infty} W(t) = 0$, which implies that the response (bottom) layer (2) reaches complete outer synchronization with the auxiliary layer (3). Consequently, the drive network (the top layer) (1) and the response network (the bottom layer) (2) realize generalized synchronization. This completes the proof. □

4 Numerical Examples

In this section, examples are presented to demonstrate the effectiveness of our established generalized synchronization method. Consider the following chaotic system

$$f_i(t, x_i(t)) = \begin{pmatrix} (25\delta + 10)(x_{i2} - x_{i1}) \\ (28 - 35\delta)x_{i1} - x_{i1}x_{i3} + (29\delta - 1)x_{i2} \\ x_{i1}x_{i2} - \dfrac{\delta + 8}{3}x_{i3} \end{pmatrix}, \tag{13}$$

where $\theta \in [0, 1]$. When $\delta = 1$, the system is the Chen system, regard it as the node dynamic system of the drive network (the top layer). When $\delta = 0$, it is the Lorenz system, take it as node dynamic system of the response (bottom) network and auxiliary system. Thus, Assumption 1 holds. Set fractional-order $\alpha = 0.98$, coupling strengths $c_1 = c_2 = 0.1$, inner-coupling matrices $H_1 = H_2 = I_3$. The two-layer networks consists of $N = 6$ nodes in each layer, the topology structure is illustrated by Fig. 1, is given as the testing network. That is, the outer-coupling matrices of the drive (top) network and response (bottom) network are

$$A = \begin{pmatrix} -3 & 1 & 1 & 0 & 1 & 0 \\ 1 & -1 & 0 & 0 & 0 & 0 \\ 1 & 0 & -1 & 0 & 0 & 0 \\ 0 & 0 & 0 & -2 & 1 & 1 \\ 1 & 0 & 0 & 1 & -3 & 1 \\ 0 & 0 & 0 & 1 & 1 & -2 \end{pmatrix},$$

$$B = \begin{pmatrix} -3 & 1 & 0 & 0 & 1 & 1 \\ 1 & -2 & 1 & 0 & 0 & 0 \\ 0 & 1 & -2 & 1 & 0 & 0 \\ 0 & 0 & 1 & -2 & 1 & 0 \\ 1 & 0 & 0 & 1 & -2 & 0 \\ 1 & 0 & 0 & 0 & 0 & -1 \end{pmatrix}.$$

Figure 2 shows the complete synchronization errors between the response network (the bottom layer) and the auxiliary system, which quickly tends to zeros. It indicates that the drive (top) network (layer) reaches inter-layer generalized synchronization with the response (bottom) network via the designed adaptive controllers (6). Thus, simulation results match the established generalized synchronization method in Theorem 1 perfectly, it is effective.

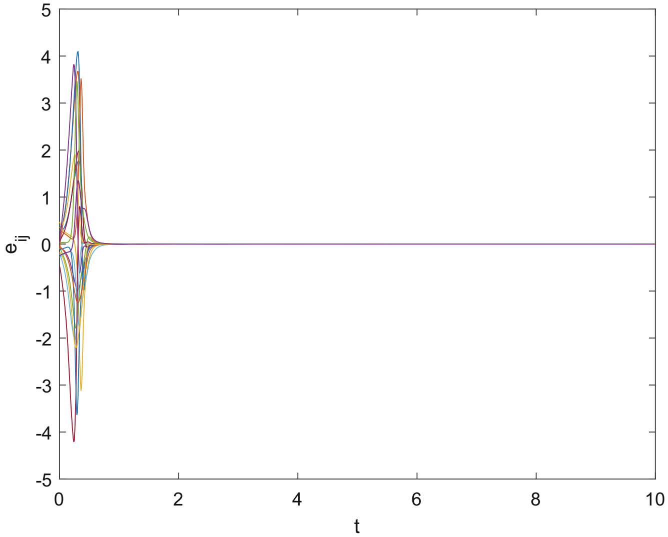

Fig. 2. Synchronization errors between the response (bottom) layer and the auxiliary system.

5 Conclusion

In this paper, inter-layer generalized synchronization for fractional-order two-layer networks has been investigated based on the auxiliary-system method. An auxiliary layer has been constructed and some adaptive controllers have been designed such that the response (bottom) network (layer) realizes complete outer synchronization with the auxiliary system. And the drive (top) network achieves inter-layer generalized synchronization with the response (bottom) network simultaneously. In addition, the effectiveness of our established generalized synchronization method has been illustrated by numerical examples.

Acknowledgments. The work was supported in part by General special scientific research plan of Shaanxi Provincial Department of Education under Grant 20JK0933, in part by Natural Science Foundation of Shaanxi Province 2023-JC-QN-0654, and in part by the National Natural Science Foundation of China under Grants 62103015, 62141604, 61621003.

References

1. Tang, Y., Qian, F., Gao, H., Kurths, J.: Synchronization in complex networks and its application: a survey of recent advances and challenge. Annu. Rev. Control. **38**, 184–198 (2014)
2. Arenas, A., Diaz-Guilera, A., Kurths, J.: Synchronization in complex networks. Phys. Rep. **469**, 93–153 (2008)
3. Lü, J., Chen, G.: A time-varying complex dynamical network model and its controlled synchronization criteria. IEEE Trans. Autom. Control **50**(6), 841–846 (2005)
4. Zhu, S., Zhou, J., Lü, J., Lu, J.: Finite-time synchronization of impulsive dynamical networks with strong nonlinearity. IEEE Trans. Autom. Control **66**(8), 3550–3561 (2021)

5. Liu, H., Li, J., Li, Z., Zeng, Z., Lü, J.: Intralayer synchronization of multiplex dynamical networks via pinning impulsive control. IEEE Trans. Cybern. **52**(4), 2110–2122 (2022)
6. Podlubny, I.: Fractional Differential Equations. Academic Press, San Diego (1999)
7. Kilbas, A.A., Srivastava, H.M., Trujillo, J.J.: Theory and Applications of Fractional Differential Equations, vol. 204. Elsevier, Amsterdam (2006)
8. Bao, H., Ju, H., Cao, J.: Adaptive synchronization of fractional-order memristor-based neural networks with time delay. Nonlinear Dyn. **82**(3), 1343–1354 (2015)
9. Liu, P., Zeng, Z., Wang, J.: Asymptotic and finite-time cluster synchronization of coupled fractional-order neural networks with time delay. IEEE Trans. Neural Netw. Learn. Syst. **31**(11), 4956–4967 (2020)
10. Liu, P., Kong, M., Zeng, Z.: Projective synchronization analysis of fractional-order neural networks with mixed time delays. IEEE Trans. Cybern. **52**(7), 6798–6808 (2022)
11. Yao, X., Liu, Y., Zhang, Z., Wan, W.: Synchronization rather than finite-time synchronization results of fractional-order multi-weighted complex networks. IEEE Trans. Neural Netw. Learn. Syst. **33**(12), 7052–7063 (2022)
12. Tong, D., Ma, B., Chen, Q., Wei, Y., Shi, P.: Finite-time synchronization and energy consumption prediction for multilayer fractional-order networks. IEEE Trans. Circuits Syst. II: Exp. Briefs (2023). https://doi.org/10.1109/TCSII.2022.3233420
13. Zhang, X., Tang, L., Lü, J.: Synchronization analysis on two-layer networks of fractional-order systems: intralayer and interlayer synchronization. IEEE Trans. Circ. Syst. I: Regular Papers **67**(7), 2397–2408 (2020)
14. Wu, X., Bao, H., Cao, J.: Finite-time inter-layer projective synchronization of Caputo fractional-order two-layer networks by sliding mode control. J. Franklin **I**(358), 1002–1020 (2021)
15. Wu, X., Bao, H.: Finite time complete synchronization for fractional-order multiplex networks. Appl. Math. Comput. **377**, 125188 (2020)
16. Luo, T., Wang, Q., Jia, Q., Xu, Y.: Asymptotic and finite-time synchronization of fractional-order multiplex networks with time delays by adaptive and impulsive control. Neurocomputing **493**, 445–461 (2022)
17. Zhou, J., Chen, J., Lü, J.: On applicability of auxiliary system approach to detect generalized synchronization in complex network. IEEE Trans. Autom. Control **62**(7), 3468–3473 (2017)

Phase Transition at Small-Medium Scales Vicsek Model Based on Eigen Microstate Method

Yongnan Jia(✉), Jiali Han, and Qing Li

University of Science and Technology Beijing, Beijing, China
ynjia@pku.edu.cn

Abstract. Vicsek Model is widely recognized as one of the classic models for studying flocking problems. The presence of discontinuous phase transitions in the Vicsek Model under vector noise has been widely recognized, while there is no accepted consensus on whether the Vicsek Model under scalar noise has discontinuous phase transitions until now. The Eigen Microstate method has been applied to study complex systems such as natural climate, and it is suitable for studying both equilibrium systems and non equilibrium systems. The method of Eigen Microstate is used in this article to study the phase transition of the Vicsek model with scalar noise at small and medium-sized scales, and concludes that the standard Vicsek model has discontinuous phase transitions. And quantitative analysis was conducted to calculate the critical point of phase transition in the standard Vicsek model, and the relationship between the critical point and cluster density was summarized.

Keywords: Vicsek Model · discontinuous phase transition · The method of Eigen Microstate

1 Introduction

Flocking phenomena can be seen everywhere in nature. Flocking phenomenon refers to the phenomenon of living or inanimate individuals gathering together, such as a flocking of bacteria [1], a shoal of fish [2,3], a flock of birds [4,5], even lifeless molecules and galaxies [6,7]. Unmanned aerial vehicle flocking and robot flocking developed from flocking phenomena are being extensively studied, and these flockings have great application value in agriculture, military, and other fields. The consistency theory of flocking is one of the most important theories supporting the collaborative control of unmanned aerial vehicle flocking, and the phase transition problem of clusters from disordered state to ordered state is of great significance for the research of unmanned aerial vehicle flocking control problems.

For the flocking phenomenon in nature, many models have been proposed to simulate this phenomenon. The earliest cluster model was the Boid model, three rules for flocking model was proposed in this model [8]. Vicsek Model was proposed on this basis in 1995 [9]. Subsequently, CuckerSmale model was

Q. Wang et al. (Eds.): CCSICC 2023, LNEE 1205, pp. 11–21, 2024.
https://doi.org/10.1007/978-981-97-3328-6_2

proposed based on Vicsek model [10,11]. They think that particles in the Vicsek model are only influenced by other particles in the velocity direction, and the magnitude of velocity is too idealized to be a constant. So improvements have made to this problem.

Through numerical simulations that interactions between individuals can lead to a new phase transition from disordered to ordered phases in [9], known as dynamic phase transition. As the simplest, most classic, and most widely used model, the Vicsek model has been extensively studied for its transition from disordered to ordered states with noise [12–15]. However, there is still some controversy regarding the critical value of the phase transition from an disordered state to an ordered state, and many scholars have conducted further research on its phase transition. The conclusion that the Vicsek model under the influence of vector noise has discontinuous phase transitions has been widely recognized [16–18], while whether the Vicsek model under scalar noise has discontinuous phase transitions has not yet been determined. Chate et al. [16] believe that the phase transition process of noise in the classical Vicsek model is discontinuous, whether it is vector noise or scalar noise. Meanwhile significant fluctuations in particle density under periodic boundary conditions was observed in this article.

Phase transition problems first appeared in the study of chemical system problems, which can be divided into discontinuous phase transition and continuous phase transition, also known as first order phase transition and Second order phase transition. Subsequently, the phase transition problem was introduced into the fields of mathematics and physics to reflect the characteristics of the system in two-phase or two-state transition. Classification of phase transition types based on whether their related order parameters undergo mutations with the change of relevant parameters. The probability histogram of order parameter occurrence, Binder increment method [19] is usually used to distinguish phase transition types.

Eigen microstate is a method for studying complex systems, which has been successfully applied in fields such as global meteorological forecasting and stock forecasting. This method takes into account the density distribution of particles and provides a more detailed description of the state of the cluster. In recent years, the fast developing eigen microstate method has been successfully applied to the study of ferromagnetic phase transition of the equilibrium Ising model [20]. It has been proven that the eigen microstate method can uniformly study the critical behavior of equilibrium and non equilibrium complex systems. Li et al. [21] applied the eigen microstate method to the Vicsek model and found discontinuous transitions in density and continuous transitions in velocity using the finite size scaling form of order parameters in the Vicsek model. Compared to the order parameters in the traditional Vicsek model, the eigen microstate method takes into account the fluctuation of particle density in the system, and its order parameters reflect the internal situation of the system more comprehensively. However, this study only focused on the larger scale Vicsek model, and there is no discussion on the phase transition problem of small and medium-sized Vicsek models. Moreover, the Vicsek model in its system is not the classic Vicsek model in reference [9].

The method of Eigen Microstate is used in this article to determine the types of phase transitions that occur in small to medium-sized Vicsek models, as scalar noise values change in the classic Vicsek model. Due to changes in noise, the transition of the Vicsek model from disorder to order is a phase transition problem. Whether the Vicsek model experiences discontinuity is determined by whether their order parameters undergo a sudden change. Vicsek model under the influence of vector noise has discontinuous phase transitions has been widely recognized, So the noise in the model in this article is scalar noise.

The organizational structure of this article is as follows: the second part of the article introduces eigen microstate method, the classic Vicsek model and experimental design is introduced in the third part, the results of the experiment and analyzes the experimental results is displayed in the fourth part, and the fifth part is the conclusion of this article.

2 Models

2.1 Standard Vicsek Model

The basic rules of the Vicsek model are as follows:

The initial velocity and position of particles are randomly distributed under two-dimensional periodic boundary conditions, and all particles in the system have a constant velocity v_0. There exists a mutual influence radius r. For any pair of particles in the system, only when the linear distance between two particles is less than r, can they have mutual influence. The direction of motion of a particle at each moment is the same as the average direction of motion of all other particles within its radius of influence at that moment.

The position of the particle at the next moment is represented as:

$$x_i(t + \Delta t) = x_i(t) + v_i(t + \Delta t)\Delta t \tag{1}$$

where $x_i(t)$ represents the position of particle i at time t, $\Delta t = 1$set the value of the constant velocity v to 0.3, The velocity of particle motion at the next moment $v_i(t + 1)$'s direction can be represented as:

$$\theta_i(t + \Delta t) = \langle\theta_i(t)\rangle_r + \eta\xi_i(t) \tag{2}$$

where $\theta_i(t)$ is a value that follow a uniform distribution in the range of $[-1/2, 1/2]$, $\eta \in [0, 2\pi]$, it indicates the magnitude of noise, namely the strength of the impact of non cluster individuals on the individual. So $\eta\xi_i(t)$ represents the angle at which particle i shifts at time t. Therein $\langle\theta_i(t)\rangle_r$ represents the average velocity direction of all neighbors of particle i (distance less than interaction radius r.

And the order parameter P is specified to indicate the degree of consistency in the particle velocity direction in the system:

$$P = \frac{1}{N}\sum_{i=1}^{N} v_i(t) \tag{3}$$

P represents the degree of consistency of particles in the flocking, used to determine whether the system is in a state of overall directional movement, with a range of $[0, 1]$. $P = 0$ indicates that the particles are in a completely disordered random state, while $P = 1$ indicates that all particles have the same velocity direction. N represents the number of particles in the flocking. The order parameter is the most commonly used to measure the degree of flocking consistency.

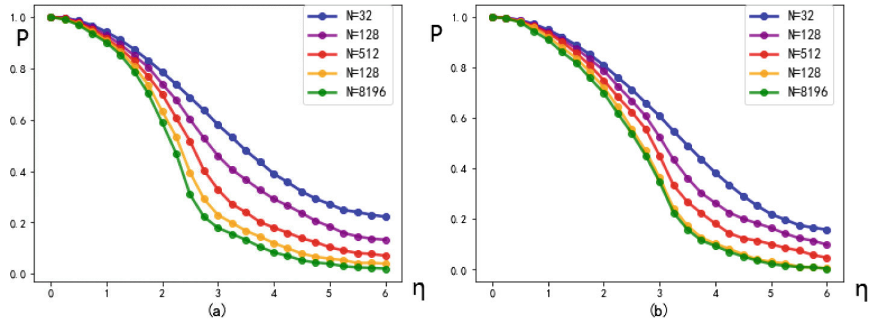

Fig. 1. The relationship between order parameters, density, and population size, (a) when $\rho = 1$ the trend of the order parameter P with scalar noise and population size. (b) when $\rho = 2$ the trend of the order parameter P with scalar noise and population size.

Figure 1 depicts the variation of the order parameter P with noise and population size at different densities, where $N = L \times L \times \rho$. L is the length of the periodic boundary. As shown in Fig. 1, the order parameters of the flocking gradually increase with the decrease of noise, and the flocking undergoes a phase transition from disorder to order. The consistency of the velocity direction of the flocking decreases with the increase of number of particles, which is consistent with the conclusion in the original text of the Vicsek model [9]. However, the order parameter only considers the consistency of particle velocity in the flocking and cannot reflect the distribution and density fluctuations of particles. However Chate et al. [16] think that the discontinuous phase transition in the Vicsek model is precisely caused by density fluctuations.

The value of σ_I in method of eigen microstate can reflect both the aggregation of particles and the density fluctuations of particles in the systems. Compared to the traditional method of using the average velocity P of particles as the order parameter, it provides a more comprehensive reflection of the system's phase transition situation.

2.2 The Method of Eigen Microstates [21]

For the equal Vicsek model, the system consists of N particles, each particle have M microstates, $s_i(t)$ represent the microstate of particle i at time t, $S(t)$

indicates the state of the entire system at time t, its specific representation is as follows:

$$S_i(t) = \begin{bmatrix} s_1(t) \\ s_2(t) \\ \vdots \\ s_n(t) \end{bmatrix} \tag{4}$$

where,

$$s_i(t) = \begin{bmatrix} \cos\theta_i(t) \\ \sin\theta_i(t) \\ \delta_{n_i}(t) \end{bmatrix} \tag{5}$$

$\theta_i(t)$ represents the angle of the velocity of particle i at time t, $\delta_{n_i}(t) = (n_i(t) - \overline{n})/\overline{n}$, the parameter reflects the distribution of neighboring particles around particle i at time t, the smaller of the $\delta_{n_i}(t)$, the closer the distribution of particle i at time t is to that of the global particles. Where

$$\overline{n} = \frac{1}{MN}\sum_{t=1}^{M}\sum_{i=1}^{N}|n_i(t)| \tag{6}$$

$v_i(t)$ represents the angle of the velocity of particle i at time t, $n_i(t)$ indicates the density of particles around particle i at time t. Where $n_i(t) = N_i(t)/2r^2$, $N_i(t)$ indicates the number of particles in a lattice with a side length of $2r$, centered around the position of particle i at time t. r represents the interaction distance between particles that affects each other. In the classic Vicsek model, r is usually set to 1, so in this system, set $r = 1$.

$$A_i(t) = \frac{s_i(t)}{\sqrt{C_0}} \tag{7}$$

where, $C_0 = \sum_{t=1}^{M}\sum_{i=1}^{N} v_i(t)^2$, represents the sum of squares of all elements in matrix A, ~~$s_i(t)$ is the element of the matrix s_i (t),~~ matrix A is $3N \times M$-dimensional matrix:

$$C = A^T \cdot A \tag{8}$$

$$K = A \cdot A^T \tag{9}$$

Matrix C and matrix K is $M \times M$-dimensional matrix and $3N \times 3N$-dimensional matrix respectively. With the eigenvectors of C and K, two unitary matrices V and U can be formed as follows:

$$V = \begin{bmatrix} v_1 \; v_2 \; \cdots \; v_M \end{bmatrix} \tag{10}$$

$$U = \begin{bmatrix} u_1 \; u_2 \; \cdots \; u_{N_T} \end{bmatrix} \tag{11}$$

Matrix V and matrix U are matrices formed by arranging the eigenvalues of matrix C and matrix K in descending order, and then arranging the eigenvectors in the order corresponding to the eigenvalues. Based on the singular value decomposition (SVD) set matrix A, matrix A can be decomposed into:

$$A = U \cdot \Sigma \cdot V^T \tag{12}$$

$$\Sigma_{IJ} = \begin{cases} \sigma_I, & I = J \leq r \\ 0, & otherwise \end{cases} \tag{13}$$

where, $r = min(M, 3N)$. Σ_{IJ} is a diagonal matrix, $\sum_{I=1}^{r} \sigma_I^2 = 1$, the sum of squares of elements on diagonal lines is 1, and the value of elements on non diagonal lines is 0, $W_I^E = \sigma_I^2$, which represents the probability of microstate u_I, when$M \rightarrow \infty$ and $N \rightarrow \infty$. If all probability amplitudes σ_I tend to 0 it indicates that the system is in a completely disordered state. If there is a probability state σ_I with a non-zero value, it indicates that there is an aggregation with the eigen microstate u_I in the system.

3 Experiment and Result

In order to make the results more accurate, when iterating the Vicsek model, the first 10000 iterations were ignored to ensure that the model had reached a stable state. To avoid continuous sampling causing high similarity between samples in adjacent time steps, this experiment conducted a sampling every 50 iterations after the system reached a stable state, with a total of 10000 samples sampled.

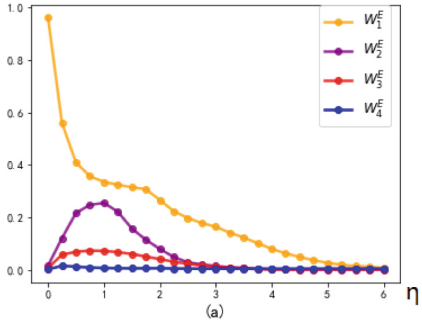

Fig. 2. At a small-medium scale and when $\rho = 1$, $N = 64$ ($L = 2^3$), the values of the first four largest eigen microstates.

Figure 2 represents when $\rho = 1$, the values of the top four eigen microstates in the small-medium scale Vicsek model, when $M \rightarrow \infty$, $W_I^4 \rightarrow 0$. So it can be concluded that under this condition, the system exhibits three aggregations similar

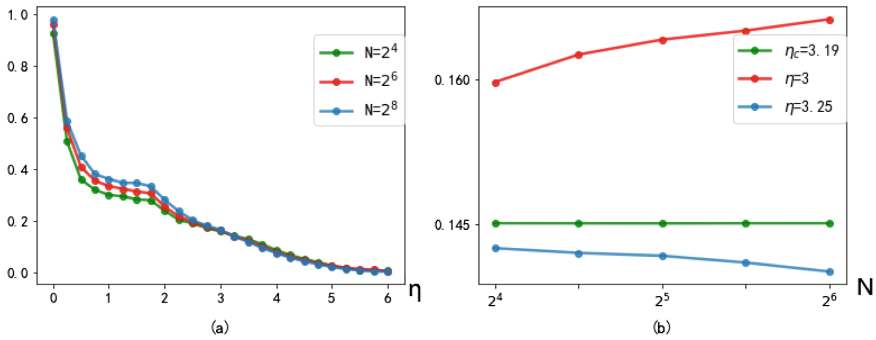

Fig. 3. When $\rho = 1$, the value of W_1^E with different system size and the critical value of phase transition for this order parameter. (a) the value of W_1^E with different system size. (b) When $\rho = 1$, the critical value of W_1^E phase transition.

to the eigen microstate, and the Vicsek model exhibits three phase transitions. This article utilizes the conclusions obtained in reference [22] to determine the critical value and type of phase transition. For formulas:

$$\sigma_I(\eta, L) = L^{(-\beta/v)} f_I(hL^{1/v}) \tag{14}$$

When $\beta = 0$, it was shown that under this noise, the value of the order parameter does not change with the change of population size in this experiment, thus it indicates that a discontinuous phase transition occurred at this phase transition point. When $\beta > 0$, it indicates that no discontinuous phase transition has occurred at that point (Fig. 3).

When this conclusion is applied to the method of eigen microstate in the Vicsek model, formula (14) can be rewritten as [21]

$$\ln W_1^E(\eta, L) = -2\beta/v \ln L + 2 \ln f_I(hL^{1/v}) \tag{15}$$

As shown in Fig. 4, it represents at a small-medium scale, and when $\rho = 1$, W_2^E, W_3^E under different population sizes do not exist a value of η make the value of $\beta = 0$ in formulation (15). Therefore W_2^E and W_3^E are continuous phase transitions.

Figure 5 shows that at a small-medium scale, and $\rho = 2$, $N = 128$, $(L = 2^3)$, the values of the first four largest eigen microstates. As shown in Fig. 6(a), the maximum eigenvalues W_1^E at different population sizes at a small scale with density of 2. As shown in Fig. 6(b), at a big scale with the density of 2, $\eta_{1c} = 3.91$ it means when $\eta = \eta_{1c}$, $\beta = 0$.

This means that the system has the same W_1^E value with different population sizes. So, it can be concluded that it is a discontinuous phase transition at this point. Therefore, it can be inferred that in the small-scale Vicsek model, there are discontinuous phase transitions with finite size effects, and the critical noise value increases with increasing density.

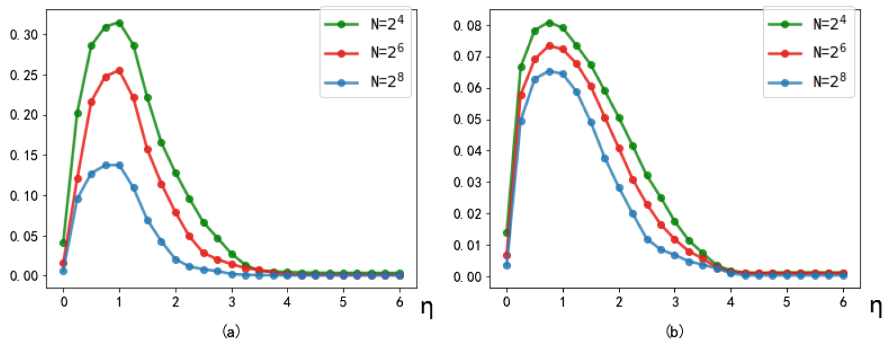

Fig. 4. At a small-medium scale and when $\rho = 1$, the variation of W_2^E, W_3^E with noise under different population sizes. (a) Changes of W_2^E with noise at different scales. (b) Changes of W_3^E with noise at different scales.

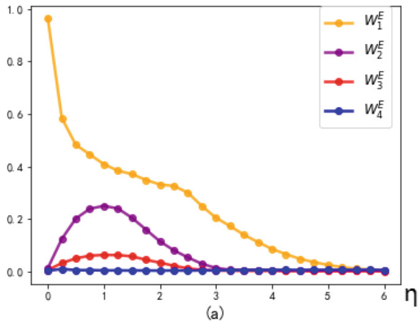

Fig. 5. At a small-medium scale and when $\rho = 2$, $N = 128$ ($L = 2^3$), the values of the first four largest eigen microstates.

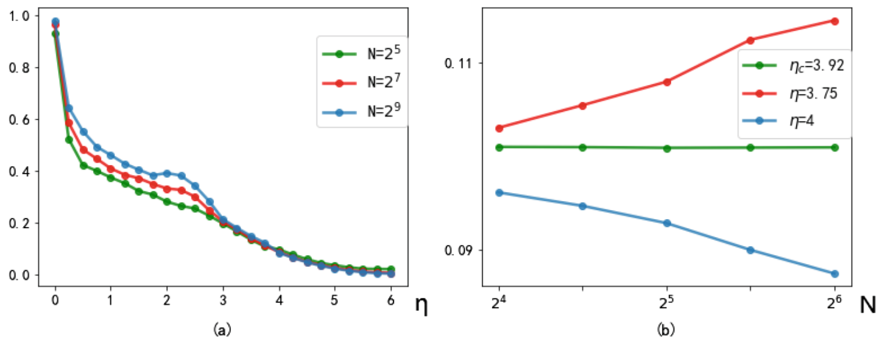

Fig. 6. When $\rho = 1$ the value of W_1^E with different system size and the critical value of phase transition for this order parameter. (a) the value of W_1^E with different system size. (b) when $\rho = 1$ the critical value of W_1^E phase transition.

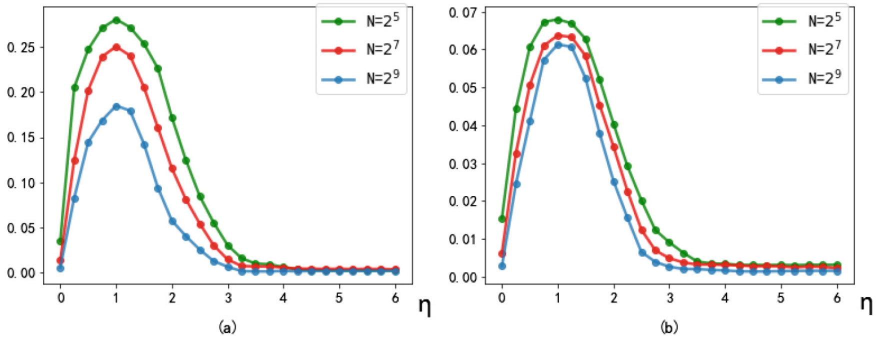

Fig. 7. At a small-medium scale and when $\rho = 2$, the variation of W_2^E, W_3^E with noise under different population sizes. (a) Changes of W_2^E with noise at different scales. (b) Changes of W_3^E with noise at different scales.

Comparing W_2^E and W_3^E under different flocking sizes, as shown in Figs. 4, 7, it can be seen that as the flocking size increases, W_2^E and W_3^E gradually decrease. Therefore, under any condition, with the change of noise η there is not a value of η to make $\beta = 0$. The phase transition they represent are both continuous phase transition.

4 Conclusion

The method of eigen microstate is used in this article to study the phase transition of the classical Vicsek model, and draw a conclusion: In the classic Vicsek model, three Bose Einstein aggregates occurred, with the same type of phase transition in both large-scale and small-medium scale Vicsek models, where discontinuous phase transitions exist. The critical value of discontinuous phase transitions increases with increasing noise, and the critical value is independent of the flocking size. Strong evidence for the viewpoint of discontinuous phase transitions in the Vicsek model in this article. However, it did not discuss the reasons for the phase transition in this article, and did not validate the Vicsek model under vector noise using the eigen microstate method. This will be our future work.

References

1. Butt, T., Mufti, T., Humayun, A., et al.: Myosin motors drive long range alignment of actin filaments. J. Biol. Chem. **285**(7), 4964–4974 (2010). https://doi.org/10.1074/jbc.M109.044792
2. Herbert-Read, J.E., Perna, A., et al.: Inferring the rules of interaction of shoaling fish. Proc. Natl. Acad. Sci. **108**(46), 18726–18731 (2011). https://doi.org/10.1073/pnas.1109355108